persion curve of the high-temperature β-phase of zirconium at ambient pressure, which has been related to the β → ω and β → α phase transitions[26]. It is therefore possible that these phonon mode softenings may play a key role in the formation of zirconium metallic glass. Inelastic scattering at elevated pressure and temperature is needed to investigate the driving mechanisms for the present observations.

Liquid–liquid phase separation or decomposition of deeply undercooled metallic liquids is at present a major problem faced in the fundamental study and technological processing of bulk metallic glasses, even for extremely good glass-formers like Vit1 ($Zr_{41.2}Ti_{13.8}Cu_{12.5}Ni_{10}Be_{22.5}$) and Vit105 ($Zr_{52.5}Ti_5Cu_{17.9}Ni_{14.6}Al_{10}$) (refs 5–8). Similarly, decomposition happens when amorphous alloys are annealed at temperatures above the glass transition temperature[5], $T_g$. Experiments have revealed that such decomposition is responsible for the embrittlement of some bulk metallic glasses[1,5]. For mechanical applications, it is important to find metallic glasses that have higher thermal stability (that is, a smaller difference between the critical temperature[1], $T_c$, and $T_g$) and thus a lower probability of decomposition. As $T_c - T_g$ reduces, however, the amorphous alloys, such as derivatives of Vit1 and Vit105, tend to have a somewhat diminished GFA. We consider that the extraordinary GFA of pure zirconium metal, combined with its superior thermal stability, will overcome the problems that exist in amorphous alloys. In addition, the glass formed within a solid state may represent a distinct state of matter that may have other distinct properties yet to be explored, which may open new opportunities for research and development in the area of metallic glasses. □

## Methods

Synchrotron X-ray experiments at high pressure and temperature were conducted on bulk, polycrystalline zirconium specimens of 1.0 mm diameter and 0.5 mm thickness, with the diffraction volume defined by 0.1 × 0.1 mm collimators. After observing the formation of amorphous zirconium, particular care was taken in our experiments, in that the formation of glassy zirconium was confirmed by collecting data at several different locations in the sample. The incident X-ray beam, however, is still too small compared to the bulk sample studied. In this regard, the GFA of bulk zirconium metal needs to be further studied by neutron diffraction.

In our high *P*–*T* neutron diffraction experiments, the cross-section of the incident neutron beam has a diameter of 5 mm, which is defined by cadmium and $B_4C$ collimators. The time-of-flight neutron diffraction patterns were collected by eight detector banks that are available for TAP-98, at a fixed Bragg angle of $2\theta = 90°$. The experiments were performed on the polycrystalline zirconium specimens of ~100 $mm^3$ sample volume. This sample size, along with the current design of high-pressure cell, limits the experimental pressure to 5 GPa at high temperatures. So, unlike our X-ray diffraction experiments, our neutron diffraction experiments did not reach the *P*–*T* conditions needed for the glassy zirconium to form. These results are mainly used to constrain the α–β phase boundary, and will be published elsewhere.

Received 5 December 2003; accepted 4 June 2004; doi:10.1038/nature02715.


1. Loffler, J. F. Bulk metallic glasses. *Intermetallics* **11,** 529–540 (2003).
2. Johnson, W. L. Bulk glass-forming metallic alloys: science and technology. *MRS Bull.* **24,** 42–56 (1999).
3. Inoue, A. Stabilization of metallic supercooled liquid and bulk amorphous alloys. *Acta Mater.* **48,** 279–306 (2000).
4. Busch, R. The thermophysical properties of bulk metallic glass-forming liquids. *J. Miner. Metals Mater. Soc.* **52,** 39–42 (2000).
5. Miller, M. K. Decomposition of bulk metallic glasses. *Mater. Sci. Eng. A* **250,** 133–140 (1998).
6. Loffler, J. F. & Johnson, W. L. Model for decomposition and nano-crystallization of deeply undercooled $Zr_{41.2}Ti_{13.8}Cu_{12.5}Ni_{10}Be_{22.5}$. *Appl. Phys. Lett.* **76,** 3394–3396 (2000).
7. Kundig, A. A., Loffler, J. F., Johnson, W. L., Uggowitzer, P. J. & Thiyagarajan, P. Influence of decomposition on the thermal stability of undercooled Zr-Ti-Cu-Ni-Al alloys. *Scripta Mater.* **44,** 1269–1273 (2001).
8. Busch, R., Schneider, S., Peker, A. & Johnson, W. L. Decomposition and primary crystallization in undercooled $Zr_{41.2}Ti_{13.8}Cu_{12.5}Ni_{10}Be_{22.5}$ melts. *Appl. Phys. Lett.* **67,** 1544–1546 (1995).
9. Wang, W. H. *et al.* Role of addition in formation and properties of Zr-based bulk metallic glasses. *Intermetallics* **10,** 1249–1257 (2002).
10. Eckert, J., Mattern, N., Zinkevitch, M. & Seidel, M. Crystallization behavior and phase formation in Zr-Al-Cu-Ni metallic glass containing oxygen. *Mater. Trans.* **39,** 623–632 (1998).
11. Busch, R., Masuhr, A., Bakke, E. & Johnson, W. L. Bulk metallic glass formation from strong liquids. *Mater. Sci. Forum* **269,** 547–552 (1998).
12. Ashby, M. F. & Jones, D. R. *Engineering Materials 2: An Introduction to Microstructures, Processing and Design* (Pergamon, Oxford, 1986).
13. Weidner, D. J., *et al.* in *High-Pressure Research: Application to Earth and Planetary Sciences* (eds Syono, Y. & Manghnani, M. H.) 13–17 (Geophysics Monograph Series, Vol. 67, American Geophysical Union, Washington DC, 1992).
14. Vaughan, M. T. *et al.* T-cup: A new high-pressure apparatus for X-ray studies. *Rev. High Press. Sci. Technol.* **7,** 1520–1522 (1998).
15. Zhao, Y., Von Dreele, R. B. & Morgan, J. G. A high P-T cell assembly for neutron diffraction up to 10 GPa and 1500 K. *High Press. Res.* **16,** 161–177 (1999).
16. Decker, D. L. High-pressure equation of state for NaCl, KCl and CsCl. *J. Appl. Phys.* **42,** 3239–3244 (1971).
17. Jayaraman, A., Klement, W. & Kennedy, G. C. Solid-solid transition in titanium and zirconium at high pressures. *Phys. Rev.* **131,** 644–649 (1963).
18. Xia, H., Duclos, S. J., Ruoff, A. L. & Vohra, Y. K. New high-pressure phase transition in zirconium metal. *Phys. Rev. Lett.* **64,** 204–207 (1990).
19. Xia, H., Ruoff, A. L. & Vohra, Y. K. Temperature-dependence of the ω-bcc phase transition in zirconium metal. *Phys. Rev. B* **44,** 10374–10376 (1991).
20. Jona, F. & Marcus, P. M. Zirconium under pressure: Structure anomalies and phase transitions. *J. Phys. Condens. Matter* **15,** 5009–5019 (2003).
21. Ostanin, S. A. & Trubitsin, V. Y. Calculation of the P-T phase diagram of Zr in different approximations for the exchange-correlation energy. *Phys. Rev. B* **57,** 13485–13490 (1998).
22. Hemley, R. J., Jephcoat, A. P., Mao, H. K., Ming, L. C. & Manghnani, M. H. Pressure-induced amorphization of crystalline silica. *Nature* **334,** 52–54 (1988).
23. Mishima, O., Calvert, L. D. & Whalley, E. Melting of ice-I at 77 K and 10 Kbar: A new method of making amorphous solids. *Nature* **310,** 393–395 (1984).
24. Highmore, R. J. & Greer, A. L. Eutectics and the formation of amorphous alloys. *Nature* **339,** 363–365 (1988).
25. Richet, P. & Gillet, P. Pressure-induced amorphization of minerals: a review. *Eur. J. Miner.* **9,** 907–933 (1997).
26. Heiming, A. *et al.* Phonon-dispersion of the bcc phase of group-IV metals 2: Bcc zirconium, a model case of dynamic precursors of martensitic transitions. *Phys. Rev. B* **43,** 10948–10962 (1991).
27. Olijnyk, H. & Jephcoat, A. P. Effect of pressure on Raman phonons in zirconium metal. *Phys. Rev. B* **56,** 10751–10753 (1997).
28. Pinsook, U. & Ackland, G. J. Calculation of anomalous phonons and the hcp-bcc phase transition in zirconium. *Phys. Rev. B* **59,** 13642–13649 (1999).


**Supplementary Information** accompanies the paper on **www.nature.com/nature**.

**Acknowledgements** This work was performed under the auspices of the US Department of Energy with the University of California. The synchrotron X-ray diffraction experiments were conducted at X17B2 beamline of NSLS and BM-13 beamline of APS, operated by COMPRES and GESCARS, respectively.

**Competing interests statement** The authors declare that they have no competing financial interests.

**Correspondence** and requests for materials should be addressed to J.Z. (jzhang@lanl.gov).

# Hydrological response to a seafloor spreading episode on the Juan de Fuca ridge

**Earl Davis[1], Keir Becker[2], Robert Dziak[3], John Cassidy[1], Kelin Wang[1] & Marvin Lilley[4]**

[1]*Pacific Geoscience Centre, Geological Survey of Canada, Sidney, British Columbia V8L 4B2, Canada*
[2]*Rosenstiel School of Marine and Atmospheric Science, University of Miami, Miami, Florida 33149, USA*
[3]*Oregon State University/NOAA, Hatfield Marine Science Centre, Newport, Oregon 97365, USA*
[4]*School of Oceanography, University of Washington, Seattle, Washington, 98195, USA*

**Seafloor hydrothermal systems are known to respond to seismic and magmatic activity along mid-ocean ridges, often resulting in locally positive changes in hydrothermal discharge rate, temperature and microbial activity, and shifts in composition occurring at the time of earthquake swarms and axial crustal dike injections[1–10]. Corresponding regional effects have also been observed[11]. Here we present observations of a hydrological response to seafloor spreading activity, which resulted in a negative formation-fluid pressure transient during and after an earthquake swarm in the sediment-sealed igneous crust of the**

**Middle Valley rift of the northernmost Juan de Fuca ridge. The observations were made with a borehole seal and hydrologic observatory originally established in 1991 to study the steady-state pressure and temperature conditions in this hydrothermally active area[12,13]. The magnitude of the co-seismic response is consistent with the elastic strain that would be expected from the associated earthquakes, but the prolonged negative pressure transient after the swarm is surprising and suggests net co-seismic dilatation of the upper, permeable igneous crust. The rift valley was visited four weeks after the onset of the seismic activity, but no signature of increased hydrothermal activity was detected in the water column. It appears that water, not magma, filled the void left by this spreading episode.**

A large seismic swarm began on 7 September 2001 in the northern part of the Middle Valley rift (Fig. 1). Initial activity was concentrated roughly 30 km north of the instrumented Ocean Drilling Program (ODP) Hole 857D, where the pressure observations presented here were made (Fig. 2). The area of activity expanded to the south along the eastern side of the valley towards the borehole site over a period of roughly ten days (Fig. 3a), then continued for a period totalling about 20 days. The total slip energy, expressed in Fig. 3b as the cumulative seismic moment, is dominated by the largest events of the swarm and is concentrated in a four-day period of time beginning five days after the swarm onset. The mechanisms for the larger events indicate a range of motion from normal to strike–slip (Fig. 1), but all are consistent with the least-compressive stress in the valley being aligned with the direction of spreading.

Changes in formation pressure observed in the borehole display a clear correlation with the seismic activity (Fig. 3b). Pressure begins to decline gradually by a few tenths of a kilopascal over the initial five days of the swarm, then drops in three discrete steps at the times of the largest earthquakes. These stepwise decreases in pressure probably reflect the elastic response of the formation in the immediate vicinity of the borehole to distant fault slip, with the size of each step (1.0, 0.8 and 2.7 kPa) being controlled by a combination of the magnitude ($M_w = 6.0$, 5.5 and 5.7, respectively) and proximity to the borehole (28, 18 and 14 km, respectively) of the corresponding earthquake. The magnitudes of local elastic strain estimated from the pressure steps are $0.3 \times 10^{-6}$, $0.2 \times 10^{-6}$ and $0.8 \times 10^{-6}$, respectively (see Methods section). Given the uncertainties in the earthquake locations and the position of the borehole relative to the nodal planes (where strain gradients are large), it is difficult to put these observations properly into the

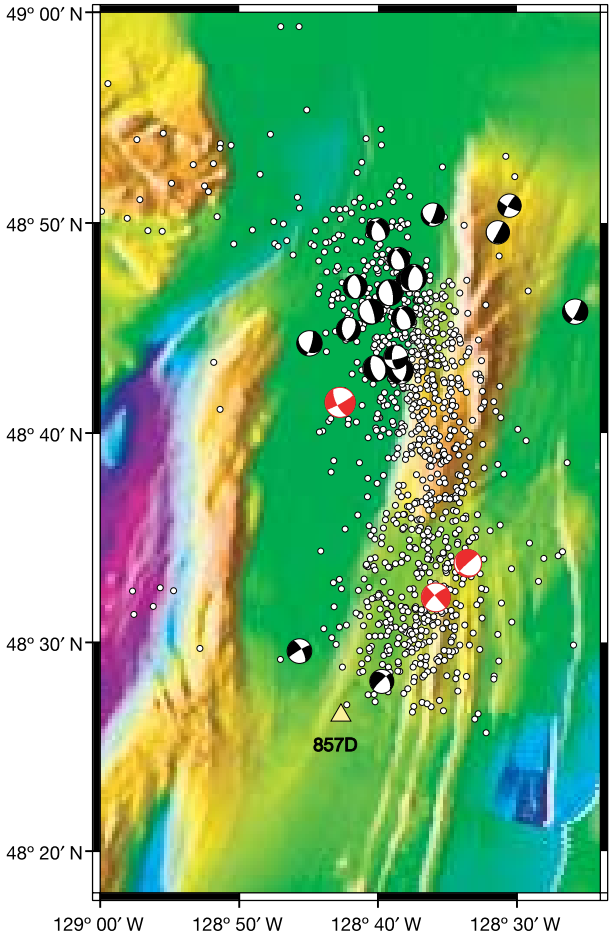


**Figure 1** Locations of events of the September 2001 seismic swarm in Middle Valley, northern Juan de Fuca Ridge, determined from offshore SoSUS hydroacoustic array tertiary-phase data (error less than 4 km)[22], along with earthquake locations determined using Western Canadian Seismic Network data (http://www.pgc.nrcan.gc.ca/seismo) and mechanisms (compressional quadrants shown solid) constrained by moment tensor solutions (J. Risteau, personal communication). Earthquakes that produced the discrete pressure steps seen in Fig. 2 are shown in red. ODP Hole 857D, located at the southern limit of the seismicity, was drilled and instrumented with a CORK borehole observatory in September 1991 to allow natural formation temperatures and pressures to be determined after drilling perturbations had dissipated[12,13]. The hole is lined with solid steel casing through unconsolidated sediments of the rift to a depth of 574 m below the seafloor (m.b.s.f.), and extends as an open hole in permeable basement to a total depth of 936 m.b.s.f.

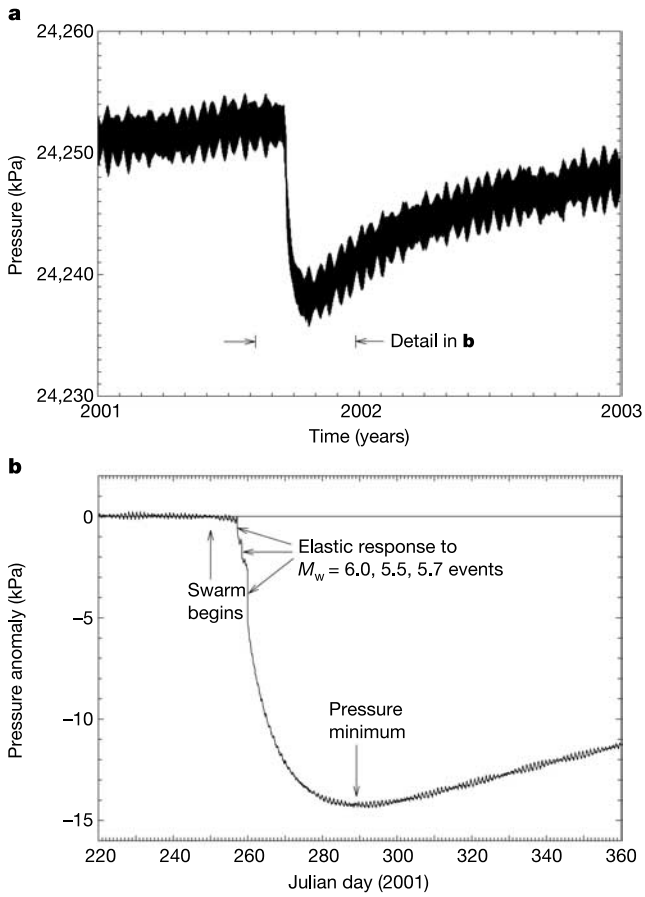


**Figure 2** Formation pressure measured hourly in ODP Hole 857D before and after the September 2001 seismic swarm. Pressures measured at the sea floor (not shown) reflect the variable load applied to the formation by the water column and atmosphere; those measured below the CORK seal at the top of the casing string reflect the average formation pressure over the open-hole interval. The total formation pressure is shown in **a**, and the anomalous pressure transient with the effects of seafloor loading removed is shown in **b**.

context of a predicted co-seismic elastic strain field, as has been done in other instances of co-seismic observations[11,14], but they do fall well within the range predicted at the site for the corresponding earthquakes using simple elastic dislocation theory[15].

Following the co-seismic elastic response, pressure continued to decrease for 30 days, reaching a minimum 14.3 kPa below the pre-swarm level (9.7 kPa below the level observed immediately after the greatest moment release; Fig. 2b), before beginning a year-long recovery towards an unperturbed state (Fig. 2a). The decrease following the swarm may reflect continuing dilatational elastic strain at the borehole site, although given the relatively large size of that portion of the anomaly and the very small seismic moment accumulated after the largest events (Fig. 3b), this would require virtually all of any later strain to have occurred without earthquakes. A more likely explanation is that the continued decline reflects lateral hydraulic diffusion through the sediment-sealed igneous crust (basement) from the earthquake source area to the borehole.

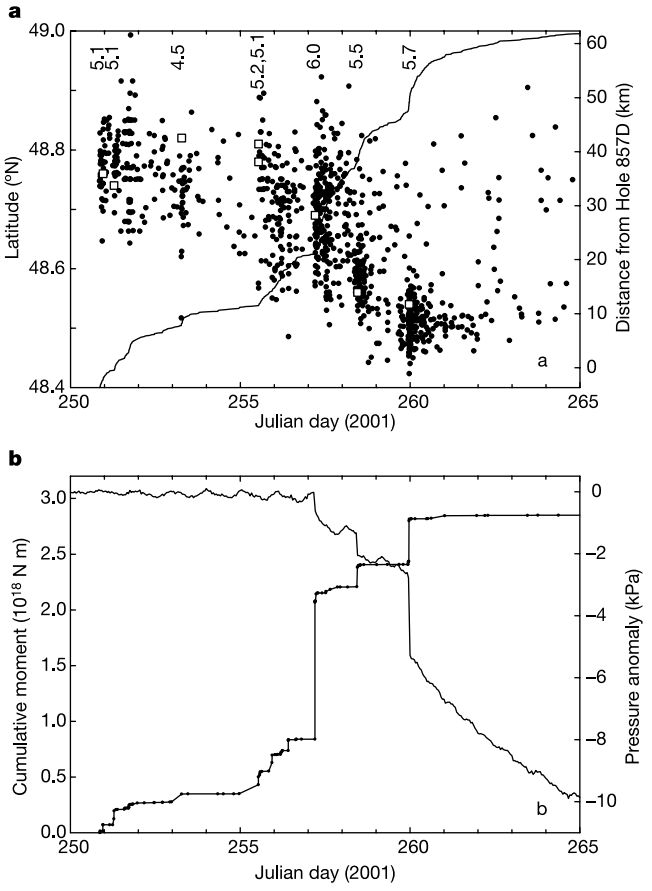


**Figure 3** Simultaneous seismic and hydrologic records of the 2001 Middle Valley earthquake swarm. Hydroacoustic (solid points) and seismic (open squares) event locations (given as distance north of ODP Hole 857D) are plotted as a function of time in **a**. The line showing the cumulative number of hydroacoustic events (totalling over 1,000 over the course of the swarm) reveals an increase and subsequent decay of the frequency of events after each large earthquake. The cumulative seismic moment (**b**, line with points) is calculated from moment magnitudes for the largest events and from body-wave magnitudes converted to moment magnitudes for intermediate events. An approximate relationship between acoustic amplitude and seismic magnitude suggests that inclusion of hydroacoustic events might add 10–20% to the total cumulative moment. Formation pressure (descending line in **b**) is shown as an anomaly relative to the average background pressure before the seismic swarm. Effects of oceanographic and atmospheric loading (see Fig. 2a) have been removed; the residual diurnal/semi-diurnal signal seen in **b** and in Fig. 2b reflects the contribution of earth tides or a diffusive (non-zero phase) ocean tidal loading component.

A simple model is considered here to explore the cause of the post-seismic pressure transient and to place a crude constraint on the hydraulic properties of the formation. The earthquake swarm is treated as a concentrated source of dilatancy located 30 km from the observation hole, with diffusion occurring axisymmetrically about a vertical line source in a fully confined permeable layer. This is directly analogous to a hydrologic 'slug test'[16] in which a sudden fluid injection or withdrawal in one borehole is monitored in an observation hole some distance away. Characteristic curves for the propagation of a pressure pulse past an observation point are shown in Fig. 4. Predicted pressures at a given range reach minima at times that depend on the hydraulic diffusivity $\eta$; given the geometry assumed, the observed 30-day transit time (Fig. 2b) suggests $\eta \approx 90\,\mathrm{m^2\,s^{-1}}$. Given reasonable formation and fluid physical properties (see Methods section), this lateral formation-scale diffusivity corresponds to a permeability of $3 \times 10^{-12}\,\mathrm{m^2}$. This value is generally consistent with borehole pumping test results completed at the time of drilling in the valley[17], and with results of numerical convection simulations[18] which require high basement permeability to yield the degree of uniformity of upper basement temperatures inferred from seafloor heat flux and seismic reflection data[19]. A crude estimate for the 'effective dilatation' associated with the source of the transient can be estimated with this same model by considering the volume of the slug of water that would need to be withdrawn at the source location to produce the magnitude of the observed pressure transient (that is, by comparing the predicted transient in Fig. 4 with the observed transient in Fig. 2). With the hydraulic diffusivity—and thus permeability and transmissivity—constrained by the diffusion time, and the maximum pressure anomaly of roughly 10 kPa (relative to the co-seismic elastic pressure anomaly) observed at a range of 30 km, a value for the ratio of the withdrawal volume (or in this application, the new pore volume created) to the layer thickness is estimated to be $V/b = 2 \times 10^4\,\mathrm{m^3\,m^{-1}}$. If this withdrawal volume is generated by dilatation along the 30-km-long portion of the axis where seismic activity is concentrated (Fig. 3), an effective 'opening' of 0.6 m is suggested. Although the numbers are not directly related, this amount of opening is comparable to the magnitude of fault slip implied by the swarm's cumulative moment, $\sim 3 \times 10^{18}$ N m. A

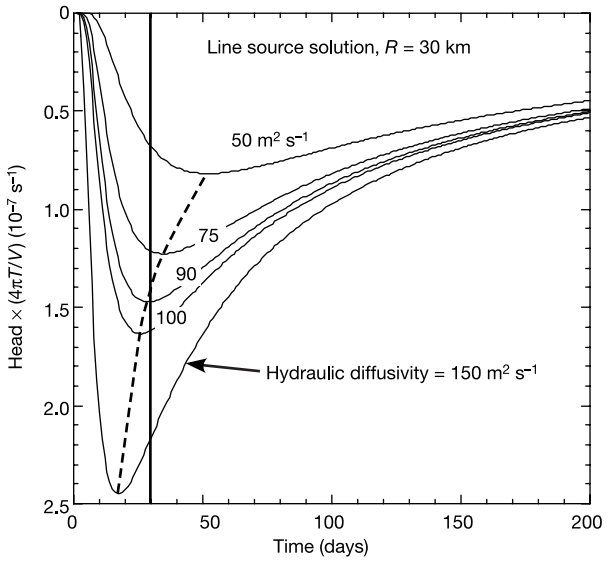


**Figure 4** Head resulting from an impulse propagating axisymmetrically in a uniform porous medium, calculated at a range of 30 km using a line-source approximation for a hydrologic slug test[16], which is valid at large distances from the source well. In the plot, head, $H = P/\rho g$, is scaled by the hydraulic transmissivity, $T = bk\rho g/\mu$ (where $b$ is layer thickness, $k$ is permeability, $\rho$ is fluid density, and $\mu$ is viscosity) and by the slug volume, $V$ (see Methods for a summary of properties).

value of roughly 1 m is suggested if the area of rupture extended over the 3-km thickness of the crust that has been observed to host microseismicity[20], and along the 30-km length of the axis defined by the concentration of seismicity seen in Figs 1 and 3. A value of 0.5 m is suggested if rupture penetrated the full thickness of the crust.

Although the general character of the predicted 'slug-test' transient (Fig. 4) is remarkably similar to that of the observed transient (Fig. 2), the results must be considered with appropriate caution, because there are large uncertainties in applying such a simple model. For example, (1) the model considers only lateral diffusion. Ventilation through the sediment section or through faults and permeable basement outcrops (as reflected by the year-long recovery to the normal formation state, established by the thermal and hydrologic structure of the valley[13]) will 'dilute' the magnitude of the initial transient, and vertical diffusion from any extension of the dilatant volume below the transmissive uppermost crust will add to and stretch the source signal. (2) Considering the dilatation to be concentrated as a vertical line-source 'implosion' is unquestionably to oversimplify. Distributed dilatancy along the axis of the valley will create diffusional directivity (enhancing propagation across strike), and reduce the effective range between the source and the observation site along axis. (3) Perhaps the greatest shortcoming of the slug-test analogue is that it does not consider the initial distribution of elastic strain associated with the spreading event, in which quadrants of contraction (and hence volumes of positive anomalous pressure) lie next to quadrants of dilatation. Diffusion between these quadrants will produce an 'annihilation' effect near nodal planes and complicate any pressure transient generated by net dilatation. Despite these uncertainties, however, the simple concentrated-source model provides a useful first-order tool for estimating net dilatation and the hydraulic transmission properties of the formation, and for guiding a more complete analysis that will take distributed co-seismic deformation and three-dimensional diffusion into account.

We note that the co- and post-seismic pressure transients observed in ODP Hole 857D represent a significant fraction (totalling nearly 20%) of the deep-seated buoyancy that drives hydrothermal discharge at a nearby vent field. A pressure differential of +80 kPa was measured across the sediment section in ODP Hole 858G, which was drilled 1.6 km to the north into a sediment-buried permeable basement edifice beneath the vent field, sealed, and instrumented at the same time as ODP Hole 857D[12,13]. Unfortunately, the seals at this high-temperature site failed long before the earthquake swarm, but it is reasonable to conclude that basement there experienced a similar co- and post-seismic reduction in pressure. The lack of any signs of augmented hydrothermal discharge searched for during a water-column investigation of the valley carried out shortly after the swarm ended is consistent with this conclusion, as well as with our primary conclusion that the permeable crust at this site suffered net dilatancy at the time of the seismic activity. □

## Methods

An outline of the relationships among strain, total stress, and pore fluid pressure in a poroelastic medium is provided in refs 11 and 21. The elastic properties involved are either established by laboratory data (at conditions corresponding to the formation temperature and pressure of 280 °C and 30 MPa, respectively), by observations of cored material, or by observed formation-fluid pressure response to tidal loading. These include: fluid compressibility, $\beta_f = 1.3 \times 10^{-9}\,\mathrm{Pa}^{-1}$; solid constituent compressibility, $\beta_s = 2.0 \times 10^{-11}\,\mathrm{Pa}^{-1}$; one-dimensional tidal loading efficiency, $\gamma = 0.14$; matrix frame compressibility, $\beta_m = 6.8 \times 10^{-11}\,\mathrm{Pa}^{-1}$; porosity, $n = 0.15$; and Poisson's ratio, $\nu = 0.25$. The resulting linear coefficient relating strain and fluid pressure is $0.29 \times 10^{-9}\,\mathrm{Pa}^{-1}$. The relationship between permeability $k$ and hydraulic diffusivity $\eta$ involves a subset of these properties plus viscosity $\mu = 10^{-4}$ Pa s (appropriate for the formation temperature): $k = \mu\xi\eta$, where $\xi$, the storage compressibility, is a function of $n$, $\beta_f$, $\beta_s$ and $\beta_m$ as outlined in ref. 21.

Received 15 January; accepted 14 June 2004; doi:10.1038/nature02755.

1. Baker, E. T. *et al.* Hydrothermal event plumes from the CoAxial seafloor eruption site, Juan de Fuca Ridge. *Geophys. Res. Lett.* **22,** 151–154 (1995).
2. Embley, R. W., Chadwick, W. W., Jonasson, I. R., Butterfield, D. A. & Baker, E. T. Initial results of the rapid response to the 1993 CoAxial event: Relationships between hydrothermal and volcanic processes. *Geophys. Res. Lett.* **22,** 143–146 (1995).
3. Von Damm, K. L. *et al.* Evolution of East Pacific Rise hydrothermal vent fluids following a volcanic eruption. *Nature* **395,** 47–50 (1995).
4. Dziak, R. P., Fox, C. G. & Schreiner, A. E. The June-July 1993 seismoacoustic event at CoAxial Segment, Juan de Fuca Ridge: Evidence for a lateral dike injection. *Geophys. Res. Lett.* **22,** 135–138 (1995).
5. Sohn, R. A., Fornari, D. J., Von Damm, K. L., Hildebrand, J. A. & Webb, S. C. Seismic and hydrothermal evidence of a cracking event on the East Pacific Rise crest near 9° 50′ N. *Nature* **396,** 159–161 (1998).
6. Delaney, J. R. *et al.* The quantum event of ocean crustal accretion: Impacts of diking at mid-ocean ridges. *Science* **281,** 222–230 (1998).
7. Dziak, R. P. & Fox, C. G. The January 1998 earthquake swarm at Axial Volcano, Juan de Fuca Ridge: Hydroacoustic evidence of seafloor volcanic activity. *Geophys. Res. Lett.* **26,** 3429–3432 (1999).
8. Lupton, J. E., Baker, E. T. & Massoth, G. J. Helium, heat, and the generation of hydrothermal event plumes at mid-ocean ridges. *Earth Planet. Sci. Lett.* **171,** 343–350 (1999).
9. Johnson, H. P. *et al.* Earthquake-induced changes in a hydrothermal system at the Endeavour Segment, Juan de Fuca Ridge. *Nature* **407,** 174–177 (2000).
10. Lilley, M. D., Butterfield, D. A., Lupton, J. E. & Olson, E. J. Magmatic events can produce rapid changes in hydrothermal vent chemistry. *Nature* **422,** 878–881 (2003).
11. Davis, E. E., Wang, K., Thomson, R. E., Becker, K. & Cassidy, J. F. An episode of seafloor spreading and associated plate deformation inferred from crustal fluid pressure transients. *J. Geophys. Res.* **106,** 21953–21963 (2001).
12. Davis, E. E., Becker, K., Pettigrew, T., Carson, B. & Macdonald, R. CORK: A hydrologic seal and downhole observatory for deep-ocean boreholes. *Proc. ODP Init. Rep.* **139,** 43–53 (1992).
13. Davis, E. E. & Becker, K. Formation temperatures and pressures in a sedimented rift hydrothermal system: Ten months of CORK observations, Holes 857D and 858G. *Proc. ODP Sci. Res.* **139,** 649–666 (1994).
14. Jonsson, S., Segall, P., Pedersen, R. & Bjornsson, G. Post-earthquake ground movements correlated to pore-pressure transients. *Nature* **424,** 179–183 (2003).
15. Okada, Y. Internal deformation due to shear and tensile faults in a half space. *Bull. Seismol. Soc. Am.* **82,** 1018–1040 (1992).
16. Cooper, H. H. Jr, Bredehoeft, J. D. & Papadopulos, I. S. Response of a finite diameter well to an instantaneous charge of water. *Wat. Resour. Res.* **3,** 263–269 (1967).
17. Becker, K., Morin, R. H. & Davis, E. E. Permeabilities in the Middle Valley hydrothermal system measured with packer and flowmeter experiments. *Proc. ODP. Sci. Res.* **139,** 613–626 (1994).
18. Bessler, J. U., Smith, L. & Davis, E. E. Hydrologic and thermal conditions at a sediment/basalt interface: Implications for interpretation of field measurements at Middle Valley. *Proc. ODP Sci. Res.* **139,** 667–678 (1994).
19. Davis, E. E. & Villinger, H. Tectonic and thermal structure of the Middle Valley sedimented rift, northern Juan de Fuca Ridge. *Proc. ODP Init. Rep.* **139,** 9–41 (1992).
20. Golden, C. E., Webb, S. C. & Sohn, R. A. Hydrothermal microearthquake swarms beneath active vents at Middle Valley, northern Juan de Fuca Ridge. *J. Geophys. Res.* **108,** doi:10.1029/2001JB000226 (2003).
21. Wang, K. Applying fundamental principles and mathematical models to understand processes and estimate parameters. In *Hydrogeology of the Oceanic Lithosphere* (eds Davis, E. E. & Elderfield, H.) (Cambridge Univ. Press, in the press).
22. Fox, C. G., Dziak, R. P., Marumoto, H. & Schreiner, A. E. Potential for monitoring low-level seismicity on the Juan de Fuca Ridge using military hydrophone arrays. *Mar. Technol. Soc. J.* **27,** 22–30 (1994).

**Acknowledgements** We acknowledge the Ocean Drilling Program for ongoing support for long-term borehole monitoring experiments, T. Pettigrew, R. Meldrum, and R. Macdonald for engineering assistance, R. Thomson and S. Mihaley for assistance with the post-swarm water-column survey on board CHS Tully, M. Fowler for assistance with SoSUS data processing, and J. Risteau for earthquake moment tensor calculations. Financial support was provided by the US National Science Foundation and by the Geological Survey of Canada.

**Competing interests statement** The authors declare that they have no competing financial interests.

**Correspondence** and requests for materials should be addressed to E.E.D. (edavis@nrcan.gc.ca).

# Cladogenesis and morphological diversification in passerine birds

**Robert E. Ricklefs**

*Department of Biology, University of Missouri-St Louis, 8001 Natural Bridge Road, St Louis, Missouri 63121-4499, USA*

**Morphological diversity tends to increase within evolving lineages over time[1,2], but the relative roles of gradual evolutionary change (anagenesis)[3] and abrupt shifts associated with speciation events (cladogenesis, or 'punctuated equilibrium')[4] have not been resolved for most groups of organisms[5]. However,**